AD-A166 650 AN EVALUATION OF A PARABOLIZED NAVIER-STOKES (PNS) CODE 1/1
FOR CONE-CYLINDER-FLARED CONFIGURATIONS(U) AIR FORCE
ARMAMENT LAB EGLIN AFB FL C J COTTRELL ET AL. APR 86
UNCLASSIFIED AFATL-TR-86-16 F/G 20/4 NL

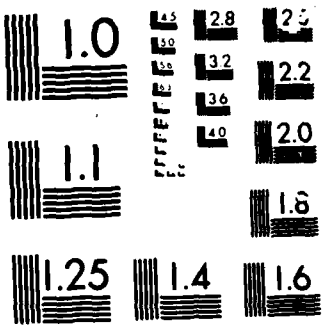

MICROCOPY CHART

UNCLASSIFIED
SECURITY CLASSIFICA

AD-A166 650

TATION PAGE

1a. REPORT SECURITY UNCLASSIFIED	1. RESTRICTIVE MARKINGS None
2a. SECURITY CLASSIFICATION AUTHORITY	3. DISTRIBUTION/AVAILABILITY OF REPORT Approved for Public Release; distribution is unlimited.
2b. DECLASSIFICATION/DOWNGRADING SCHEDULE	
4. PERFORMING ORGANIZATION REPORT NUMBER(S) AFATL-TR-86-16	5. MONITORING ORGANIZATION REPORT NUMBER(S)
6a. NAME OF PERFORMING ORGANIZATION Air Force Armament Lab	6b. OFFICE SYMBOL (If applicable) DLCA
6c. ADDRESS (City, State and ZIP Code) Eglin AFB FL 32542-5000	7a. NAME OF MONITORING ORGANIZATION
8a. NAME OF FUNDING/SPONSORING ORGANIZATION Air Force Armament Lab	8b. OFFICE SYMBOL (If applicable) DLCA
8c. ADDRESS (City, State and ZIP Code) Eglin AFB FL 32542-5000	7b. ADDRESS (City, State and ZIP Code)
	9. PROCUREMENT INSTRUMENT IDENTIFICATION NUMBER

10. SOURCE OF FUNDING NOS.			
PROGRAM ELEMENT NO. 61102F ~~61021~~	PROJECT NO. 2307	TASK NO. E1	WORK UNIT NO 25

11. TITLE (Include Security Classification) An Evaluation of a Parabolized Navier-Stokes (PNS) Code for Cone-~~Cylinder Flared Configurations~~

12. PERSONAL AUTHOR(S)
Charles J. Cottrell, Gary T. Chapman

13a. TYPE OF REPORT	13b. TIME COVERED	14. DATE OF REPORT (Yr., Mo., Day)	15. PAGE COUNT
Final	FROM Oct 82 TO May 84	1986 April	11

16. SUPPLEMENTARY NOTATION
Availability of this report is specified on verso of front cover.

17. COSATI CODES		
FIELD	GROUP	SUB. GR
20	04	
16	02	

18. SUBJECT TERMS (Continue on reverse if necessary and identify by block number)
computational fluid dynamics, separated flow, supersonic freestream aerodynamic prediction

19. ABSTRACT (Continue on reverse if necessary and identify by block number)
A PNS code's capability to predict the onset of laminar and turbulent boundary layer separation, forces, moments, and pressure distributions was investigated. Predictions of incipient separation show good agreement with experimental results. Force and moment calculations were found to agree favorably with experimental data for a wide range of geometries for Mach numbers from 2 to 4 with turbulent boundary layers. Limited comparison of pressure distribution data also showed good agreement. Skin friction and Stanton number calculations are presented to indicate the code's capability to calculate this information and hence, provide a complete data base for attached flow conditions. The sensitivity of these calculations to smoothing and marching parameter variations was examined and found to be acceptable for most design work. The code was found to be suitable to complement or reduce wind tunnel experimentation for the design of this class of configuration with regard to accuracy, cost and usability.

20. DISTRIBUTION/AVAILABILITY OF ABSTRACT	21. ABSTRACT SECURITY CLASSIFICATION
UNCLASSIFIED/UNLIMITED ☒ SAME AS RPT ☒ DTIC USERS ☐	UNCLASSIFIED

22a. NAME OF RESPONSIBLE INDIVIDUAL	22b. TELEPHONE NUMBER (Include Area Code)	22c. OFFICE SYMBOL
CHARLES J. COTTRELL	(904) 882-5652	AFATL/DLCA

DTIC ELECTE APR 11 1986 E

DD FORM 1473, 83 APR EDITION OF 1 JAN 73 IS OBSOLETE

UNCLASSIFIED
SECURITY CLASSIFICATION OF THIS PAGE

DTIC FILE COPY

AN EVALUATION OF A PARABOLIZED NAVIER-STOKES (PNS) CODE FOR CONE-CYLINDER-FLARED CONFIGURATIONS

Charles J. Cottrell*
U. S. Air Force Armament Laboratory
Eglin Air Force Base, Florida 32542

Gary T. Chapman**
NASA Ames Research Center
Moffett Field, California 94035

Abstract

A PNS code's capability to predict the onset of laminar and turbulent boundary layer separation, forces, moments, and pressure distributions was investigated. Predictions of incipient separation show good agreement with experimental results. Force and moment calculations were found to agree favorably with experimental data for a wide range of geometries for Mach numbers from 2 to 4 with turbulent boundary layers. Limited comparison of pressure distribution data also showed good agreement. Skin friction and Stanton number calculations are presented to indicate the code's capability to calculate this information and hence, provide a complete data base for attached flow conditions. The sensitivity of these calculations to smoothing and marching parameter variations was examined and found to be acceptable for most design work. The code was found to be suitable to complement or reduce wind tunnel experimentation for the design of this class of configuration with regard to accuracy, cost and usability.

Nomenclature

A = reference area

C_f = skin friction coefficient, $2\tau_W/\rho_\infty u_\infty^2$

C_m = pitching moment coefficient about model tip, (moment)/1/2 $\rho_\infty u_\infty^2 Ad$

C_N = normal force coefficient, (normal force)/1/2$\rho_\infty u_\infty^2 A$

C_{m_α} = initial pitching moment curve slope, $\frac{\partial C_m}{\partial \alpha}$, per deg.

C_{N_α} = initial normal force curve slope, $\frac{\partial C_N}{\partial \alpha}$, per deg.

C_p = pressure coefficient, $(P-P_\infty)/1\ 2\rho_\infty u_\infty^2$

C_p = specific heat at constant pressure

d = cylinder diameter

$\ell_{cn}+\ell_{cy}$ = length of cone-cylinder combination,

ℓ = total body length

ℓ_{cn} = length of cone

ℓ_{cy} = length of cylinder

ℓ_f = length of flare

M_∞ = freestream Mach number

P_∞ = freestream pressure

P = ~~freestream~~ pressure

Q_W = wall heating rate

Re_L = $(\rho_\infty u_\infty L)/\mu_\infty$

St = Stanton number, $Q_W/\rho_\infty u_\infty c_p(T_W - T_t)$

T_t = total temperature

T_W = wall temperature

u_∞ = axial component of freestream velocity

x = axial location

α = angle of attack

θ_c = cone half angle

θ_f = flare angle

μ_∞ = freestream viscosity

ρ_∞ = freestream density

τ_W = axial component of wall shear

ϕ = circumferential angle

*Aerospace Engineer, Aeromechanics Division, Member AIAA
**Senior Staff Scientist, Thermo- and Gas Dynamics Division, Member AIAA

I. Introduction

There are an abundance of technical papers in the literature concerning the application of PNS codes to various configurations; see, for example, References 1-7. A summary of PNS work is given in Reference 8. Some of these papers address the flow about flaps and flares[1-3]. Others address the flow about boattails[5-7]. However, little effort has been made to assess the accuracy, cost effectiveness, and usability of a PNS code for a complete set of data that might be used to design a relatively simple aerodynamic shape, such as a cone-cylinder-flared projectile. Further, there has been little effort to establish the limits of a PNS code in predicting incipient (onset of) separation with regard to flap or flare design. The parabolic nature of the PNS (marching) codes causes them to diverge or "blow up" when flow velocities opposite to the marching direction are encountered[3]. However, it has not been established that this divergence corresponds to

incipient separation determined from experimental data.

The purpose of this paper is twofold. The first purpose is to assess the ability of a PNS code to accurately detect the onset of separation. The second purpose is to provide a set of calculations for cone-cylinder-flared bodies of revolution, compare them to experimental results, and make an assessment of the suitability of PNS calculations to supplant or replace wind tunnel testing including accuracy and cost effectiveness. In the next two sections a brief description of the PNS code and the configurations and flow conditions considered for both the separation and aerodynamic studies will be presented. In the third section, typical results will be examined and discussed for each study, and finally, major conclusions will be given.

II. PNS Code Description

The code chosen for this study was developed to solve the steady-state, ideal gas, high Reynolds number, thin layer, parabolized Navier-Stokes equations[9-11]. This marching code is based on a non-iterative technique formulated by Schiff and Steger which uses the Beam and Warming implicit finite-difference relations and the alternating direction implicit algebraic equation solver[12,13].

The initial code was modified by Chaussee et al.,[2,9-11] to solve for the flow field around configurations with blunt tips by using in-flow data starting planes generated from a full Navier-Stokes code. The present form of the code expands the work started by Chaussee et al., to include refinements in the prediction procedure involving grid generation, boundary conditions, and increased numerical stability[14]. When flows with turbulent boundary layers are considered, the Baldwin-Lomax algebraic two layer turbulence model is employed to calculate the turbulent eddy viscosity[15].

All PNS flow field solutions were obtained by marching from an externally supplied starting solution one half cylinder diameter aft of the conical nose vertex. An algebraic grid measuring 19 by 45 points in the circumferential and radial directions, respectively, was employed. Thirty five of the 45 radial grid points were clustered near the wall to resolve the boundary layer. An axial marching step size of .025 cylinder diameters was employed up to a plane one cylinder diameter aft of the cone-cylinder juncture. This small step size was necessary to capture the strong gradients in the flow field that occur in the shoulder region. The step size was then relaxed to 0.1 diameters while marching along the cylinder to a plane 0.6 diameters upstream of the cylinder-flare juncture. The step size was then reduced to .025 diameters to accommodate the accompanying rapid pressure rise. This step size was approximately one fourth the boundary layer thickness in this region. Previous work done by Viegas and Horstman indicates that a step size on the order of half a boundary layer thickness is sufficient to resolve two-dimensional shock/boundary layer interactions[19]. Nominal values of the code's smoothing and damping parameters were 0.2 with the exception of the implicit smoothing parameter which was 0.40. The nominal value of the grid spacing parameter at the wall was .0001. Any exceptions to these parameters will be noted in the text.

III. Configurations and Flow Conditions

To meet this paper's first objective, the separation study, a 10° cone-cylinder-flare (Fig. 1) was examined at a freestream Mach number of 5 to determine the capability of the PNS code to detect the onset of flow separation induced by shock/boundary layer interaction at the cylinder-flare junction. The flare angle and Reynolds number were varied to examine the relationship among flow and geometry parameters regarding the onset of separation. Incipient separation was investigated under both laminar and turbulent conditions. The laminar unit Reynolds number was varied from 1.5×10^5/in. to 4.0×10^5/in. The turbulent range was taken from 7.0×10^5/in. to 1.5×10^6/in. All cases were run for a wall temperature of 520° R and a freestream temperature of 432° R.

To address the second objective, the aerodynamic study, several cone-cylinder-flared configurations (Fig. 1) have been examined. These configurations were identical to those tested in a wind tunnel study in the mid 1950s[16-18]. PNS results are presented for Mach numbers of 2.18, 2.81, and 4.04 at unit Reynolds numbers of 5.0×10^5/in., 6.0×10^5/in., and 4.0×10^5/in., respectively. Fully turbulent flow was assumed for all conditions. All cases were run for a freestream total temperature of 542° R and a wall temperature of 527° R. This wall temperature is very near adiabatic conditions. An adiabatic wall condition was tried, but the code failed to march on to the 20° flare. However, the code successfully marched over a 5° flare under these conditions.

IV. Results and Discussion

A. Separation Study

The separation study with its objective of determining the ability of the PNS code to detect incipient separation was accomplished for a given Reynolds number by gradually increasing the flare angle until the code indicated separation had occurred, and then comparing the results with experimental data. These results are compared in Fig. 2 with experimental two-dimensional ramp data on incipient separation correlated by Needham and Stollery[20]. To first order the flare appears as a two-dimensional ramp to the PNS code. The PNS code provides reasonable estimates for the condition of incipient separation. For the case of laminar flow, separation is indicated at slightly higher flare angles than occurred for the experimental data on two-dimensional ramps. The trend with Reynolds number closely follows the experimental data. For turbulent flow, separation occurs at a slightly lower flare angle than the two-dimensional data would indicate. The affect on indicated separation caused by variations in the code's smoothing parameters was examined and is summarized in Table 1. The results indicate that a decrease in the incremental smoothing

parameters causes the code to register axial separation at lower flare angles. This is consistent with the purpose of these parameters to augment the axial velocity component so that isolated small negative axial velocities will not arbitrarily preclude further marching. Similarly, results indicate that a decrease in the explicit and implicit artificial viscosity smoothing parameters causes the code to indicate separation at higher flare angles. It is not completely understood why this latter affect is present. In conclusion, using the nominal values of the smoothing parameters, reasonable estimates of incipient separation can be obtained.

B. Aerodynamic Study

Over fifty different cases were calculated to verify the code's suitability to predict flow field and aerodynamic force and moment variations due to changing geometric parameters and freestream Mach numbers. This number of cases was sufficient to obtain an estimate for the cost of computing a complete data matrix as in the wind tunnel tests[16-18] and to obtain an assessment of the utility of the code.

Typical force and moment results are shown in Figs. 3-10. Variations of normal force coefficient and pitching moment coefficient with angle of attack are compared with the experimental data in Figs. 3-4. Variation of initial normal force curve slope and initial pitching moment curve slope with flare angle and flare length are compared with the experiment in Figs. 5 and 6. Variations of normal force curve slope and pitching moment curve slope with cylinder length and Mach number, as well as comparison with experimental data, are presented in Figs. 7-10. A typical axial distribution of the pressure coefficient for both the windward and leeward rays at 2° angle of attack is presented and compared with experimental data in Fig. 11. Circumferential distributions at three axial locations are given in Fig. 12. Similar axial and circumferential distributions for skin friction coefficient and Stanton number for the same conditions are presented in Figs. 13-16; however, experimental data were not available for comparison.

Figures 3-10 demonstrate basic force and moment results for parametric variations normally encountered in a design process. All of the results show good agreement with experimental data. The absolute values of the calculations are slightly higher than the corresponding experimental data (as much as ten to fifteen percent for large flare angles and angles of attack). However, the accuracy achieved is sufficient for most design work. As one would expect, larger flares produce larger normal force curve slopes and pitching moment curve slopes. This is evident in Figs. 5 and 6 for both flare length and flare angle. Generally, the affect of a longer cylinder length is to decrease C_{N_α} (Fig. 7). This is a result of so called "lift carry over"[21] which refers to the significant circumferential pressure difference around short cylinders at angle of attack. This pressure difference is converted into additional lift on the flare above that which the flare would generate if the pressure was more uniform around the cylinder, which is the case for the longer cylinders ($\ell_{cy}/d = 4.0$). Hence, the curves in Fig. 7 are flattening out with increased ℓ_{cy}/d. The affect of cylinder length on C_{m_α} is much more dramatic and direct. Although there is a slight decrease in C_{N_α} with cylinder length as just discussed, the primary affect on C_{m_α} is to increase the moment arm. Hence, C_{m_α} increases almost linearly with ℓ_{cy}/d (Fig. 8). In Figs. 9 and 10 the Mach number trends are the same as one would obtain on cones (Ref. 22, Chart 8). C_{N_α} and C_{m_α} decrease with Mach number for $\theta_f = 5^{\circ}$. However, both coefficients increase with Mach number for $\theta_f = 20^{\circ}$.

Drag coefficients were not measured in References 16-18; however, a comparison with experimental data at $M_\infty = 3.0$ on a 20° flare[23] shows good agreement:

$$C_{D_{experiment}} = 2.22 \quad , M_\infty = 3.0$$

$$\theta_c = 22.5 \ , \quad \ell_{cy}/d = 4, \quad \ell_f/d = 2.4$$

$$C_{D_{computation}} = 2.19 \quad , M_\infty = 2.81$$

This is not surprising since the total drag is dominated by wave drag (base drag is not included), and the pressure distribution shown in Fig. 11, to be discussed next, agrees quite well with the experiment.

Figure 11 demonstrates the generally good agreement between the computed and experimental axial pressure coefficients, with the experimental data being slightly higher than the computations. Fig. 12 shows the circumferential distribution of pressure coefficients. The distributions immediately upstream of the flare ($x/\ell = 0.50$) and at the flare's base ($x/\ell = 1.0$) show the expected steady decrease in pressure from windward to leeward, although the variation just before the flare is very small. The distribution just after the cylinder-flare junction ($x/\ell = 0.54$) begins with this trend, but the pressure starts to rise again as it approaches the leeward side ($\phi \approx 70^{\circ}$) and then stabilizes. This suggests the possibility that circumferential separation is beginning to occur. Circumferential separation, if present, is not very strong since there is no evidence of it further back on the flare. (Though not included in the results, a long cone-cylinder configuration was examined at these flow conditions and showed strong evidence of circumferential separation.) It should be noted that this 20° flare angle is very near incipient separation, as can be deduced from Fig. 2. This is supported by the fact that the experimental pressure distribution (Fig. 11) also shows a slight pressure rise starting at approximately $x/\ell = 0.48$. The computed results for skin friction and Stanton number for this case also indicate that the boundary layer is close to incipient axial separation.

The axial and circumferential distributions of the skin friction coefficient are presented in Figs. 13 and 14, respectively. An examination of Fig. 13 reveals that skin friction varies smoothly with axial position except in the vicinity just downstream of the flare junction.

The flow expansion at the cone/cylinder shoulder increases the boundary layer thickness resulting in a rapid decrease in skin friction coefficient which then steadies to a slow decline as one expects of a turbulent boundary layer. The sudden increase in the skin friction coefficient at the flare junction is physically unreal and is a result of the parabolic nature of the equations. In the real flow the pressure rise is felt forward of the flare junction, allowing the flow to gradually decelerate reducing the skin friction ahead of the flare with a further rapid decrease on the first position of the flare. The existence of the negative value of skin friction can be misleading since the code's smoothing parameters produce the necessary stabilization under these conditions. However, it does indicate that the 20° flare is very close to axial separation. The flow finally stabilizes, and the skin friction coefficient on the flare resumes its steady decline. As expected, the skin friction is higher here than on the cylinder because of the thinner boundary layer on the flare. The circumferential distributions at $x/\ell = 0.50$ and $x/\ell = 1.0$ vary smoothly, reflecting the thinner boundary layer on the windward side (higher C_f) and thicker boundary layer on the leeward side (lower C_f); see Fig. 14. The distribution at $x/\ell = 0.54$ is not as uniform and reflects the fact that there is some circumferential separation occurring immediately downstream of the flare junction. Details of this curve and similar curves in the region between $x/\ell = 0.52$ and 0.60 should not be taken as absolute but do indicate boundary layer trends and the nearness of axial separation.

Figures 15 and 16 respectively show the axial and circumferential Stanton number. The computed values result from the wall temperature being set slightly higher than the wall's recovery temperature under adiabatic conditions ($T_W = 527^{\circ}$ R). Hence, in general the heat transfer is from the wall to the flow which results in a negative Stanton number over much of the body (Fig. 15). Exceptions occur downstream of the cone-cylinder shoulder and downstream of the flare junction. At the shoulder, the boundary layer is cooled by the expansion and greatly thickened. The cooling would tend to make the heat transfer more negative, and the thickening would reduce the magnitude. Neither would change the sign as indicated. Therefore, the change in sign is not fully understood and may be a result of the parabolic nature of the equations. Downstream of the flare junction the compression heats the flow increasing the air temperature, and the boundary layer becomes thinner due to the pressure rise. The compression is sufficient to change the sign of the heat transfer. The thinning of the boundary layer would increase the magnitude. Neither, however, are sufficient to explain the very high Stanton number immediately after the flare junction. Again, this spike may be a result of the parabolic nature of the equations. Further downstream of the junction, the flow rapidly adjusts and resumes its negative Stanton number level. The circumferential variation tends to be smooth at the $x/\ell = 0.50$ and 1.0 locations, being slightly more negative on the windward side where the boundary layer is thinner (Fig. 16). However, at $x/\ell = 0.54$ a change in the Stanton number near $\phi \approx 70^{\circ}$ is evident. Again, this is associated with a possible circumferential separation.

A very brief study was conducted to determine the sensitivity of results to code inputs such as smoothing parameters, marching step size, and grid spacing in the boundary layer. The affect of smoothing parameters on axial separation has been discussed previously. The force and moment results were only weakly affected by these parameters, on the order of a few percent or less. All the distributions were likewise only slightly affected except in the region of shock/boundary layer interaction near the junction of the flare, particualarly the 20° flare angle case where the flow is near separation. In this area significant affects were present. The pressure coefficient varied by thirty to forty percent near the maximum C_p, and the oscillations that occurred did not dampen out immediately. The greatest sensitivity due to the variation of these parameters occurred with the skin friction coefficient in this same region. This is not as critical in one sense, because skin friction is not an important contribution to drag. However, the skin friction curves may be the best indicator of how close to separation the flow is, rather than relying on the PNS code failing as a criteria. To summarize, the sensitivity study, although brief, indicated that basic design data, such as forces and moments, are insensitive to the above parameters as are the distributions of pressure, skin friction, and Stanton number, except in the region of a rapid geometry change. However, in a region of rapid geometry change such as the flare junction, results are sensitive to these parameters, and the user should conduct his own sensitivity studies.

C. Evaluation of Usability

It is not sufficient that the PNS code provide accurate results. The code must do so in a cost effective fashion as well as provide results in a timely and flexible manner to impact the engineering design of an airframe. In discussing the cost and usability of the code, two sets of factors must be remembered. First, the results were generated on a medium size computer, a CDC Cyber 176. Second, the users, in this case the authors, are not computational experts but users of codes for aerodynamic research and analysis along with other available tools, both experimental and analytic.

It is estimated that a complete computational data matrix comparable to that of the wind tunnel test of Ref. 16-18 could be obtained at one sixth the cost of a wind tunnel test today. This computational estimate includes a small factor to cover geometry initiation and errors in data entry. The computational cost also reflects maximum use of restarts using stored data planes generated from previous calculations. This factor of six is considered to be a conservative estimate, because the low computer cost, flexibility, and short response time (on the order of a few hours) for the computation would allow a more efficient approach to the design process. With this flexibility and short response time only a skeleton matrix would be

computed to determine basic trends such as have been illustrated here. A preliminary design could be developed from these trends, and from then on, only limited computations would be performed as the design matured. Because of scheduling constraints this approach is nearly impossible with a wind tunnel. One final factor that needs to be considered in the cost analysis is that the calculations provide not only the forces and moments, but the entire flow field including skin friction, heat transfer and pressure distributions at no additional cost. Normally, separate tunnel entries would have to be made for each, or, in many cases the designer might have to do without skin friction, heat transfer, or pressure distribution results. This additional information can lead to a more complete design and one in which there is more confidence because of that completeness. When all of these factors are taken into account the cost of design by computation of these simple bodies with attached flow is an order of magnitude less costly than for wind tunnel testing. In addition, as is noted in Reference 24, the two factors of flexibility and increased confidence are of more importance than cost in many cases. These factors impact other areas of the design and hence can reduce the overall design cycle time and thus reduce overall cost.

V. Concluding Remarks

Based on calculations with a PNS code of a large number of cone-cylinder-flared configurations at several Mach numbers and Reynolds numbers under attached flow conditions the following conclusions can be drawn.

The PNS code examined provided flow field and aerodynamic force and moment data of sufficient accuracy for general design of this class of configurations. The PNS code provided reasonable estimates for the onset of separation on flared bodies and hence, can be used as a tool to establish the design limits for attached flow. The PNS calculations are a very cost effective approach for the design of cone-cylinder-flared configurations with attached flow.

References

1. Hung, C.M. and Chaussee, D.S., "Computation of Supersonic Turbulent Flows Over an Inclined Ogive-Cylinder-Flare," AIAA Journal, Vol. 19, Sep 81, pp. 1139-1144.

2. Chaussee, D.S., Patterson, J.L., Kutler P., Pulliam, T., and Steger, J.L., "A Numerical Simulation of Hypersonic Viscous Flows over Arbitrary Geometries at High Angle of Attack," AIAA Paper 81-0050, St. Louis MO, Jan 81.

3. Chaussee, D.S. and Rizk, Y.M., "Computation of Viscous Hypersonic Flow over Control Surfaces," AIAA Paper 82-0291, Orlando FL, Jan 82.

4. Lin, S. and Rubin, S.G., "Three-Dimensional Supersonic Viscous Flow Over a Cone at Incidence," AIAA Journal, Vol. 20, No. 11, Nov 82, pp. 1500-1507.

5. Schiff, L.B. and Sturek, W.B., "Numerical Simulation of Steady Supersonic Flow Over an Ogive-Cylinder-Boattail Body," AIAA Paper 800066, Pasadena CA, Jan. 80.

6. Sturek, W.B. and Nylin, D.C., "Computational Study of the Magnus Effect on Boattailed Shell," AIAA Journal , Vol. 20, No. 10, Oct. 82, pp. 1462-1464.

7. Sturek, W.B. and Schiff, L.B., "Numerical Simulation of Steady Supersonic Flow over Spinning Bodies of Revolution," AIAA Journal , Vol. 20, No. 12, Dec. 82, pp. 1724-1731.

8. Rubin, S.G., "A Review of Marching Procedures for Parabolized Navier-Stokes Equations," Symposium on Numerical and Physical Aspects of Aerodynamic Flows, California State Univ., Long Beach CA, Jan 81.

9. Chaussee, D.S., Kutler, P., and Pulliam, T. H., "Three-Dimensional Viscous Flow Field Program: Part 1, Viscous Blunt Body Program (Interim Report)," AFWAL-TM-81-63-FIMG, Mar 81.

10. Chaussee, D.S. and Steger, J.L., "Three-Dimensional Viscous Flow Field Program: Part 2, A Curvilinear Grid and Body Generation Program for Generalized Configurations (Interim Report)," AFWAL-TM-81-64-FIMG, Mar 81.

11. Chaussee, D.S. and Steger, J.L., "Three-Dimensional Viscous Flow Field Program: Part 3, Parabolized Navier-Stokes Program Interim Report," AFWAL-TM-81-65-FIMG, Mar 81.

12. Schiff, L.B. and Steger, J.L., "Numerical Simulation of Steady Supersonic Viscous Flow," AIAA Journal, Vol. 18, Dec 80, pp. 1421-1430.

13. Beam R. and Warming, R.G., "An Implicit Factored Scheme for the Compressible Navier-Stokes Equations," AIAA Journal, Vol 16, Apr 78, pp. 393-402.

14. Shanks, S.P., Srinivason, G.R., and Nicolet, W.E., "AFWAL Parabolized Navier-Stokes Code: Formulation and User's Manual," AFWAL-TR-82-3034, Jun 82.

15. Baldwin, B.S. and Lomax, H., "Thin Layer Approximation and Algebraic Model for Separated Turbulent Flows," AIAA Paper 78-257, Huntsville AL, 78.

16. Sims, J.L. and Henderson, J.H., "Normal Force, Pitching Moment, and Center of Pressure of Eighty Cone-Cylinder-Frustum Bodies of Revolution at Mach Number 2.81," Department of the Army Ordnance Corps Report No. 6R3N2, Redstone Arsenal, Mar 56.

17. Henderson, J.H. and Sims, J.L., "Normal Force, Pitching Moment, and Center of Pressure of Eighty Cone-Cylinder-Frustum Bodies of Revolution at Mach Number 4.04," Department of the Army Ordnance Corps Report No. 6R3N1, Redstone Arsenal, Mar 56.

18. Lavender, R.E., Henderson, J.H., and Deep, R.A., "Normal Force, Pitching Moment, and Center of Pressure of Eighty Cone-Cylinder-Frustum Bodies of Revolution at Mach Numbers 2.46 and 4.04," Department of the Army Ordnance Corps Report No. 6R3N3, Redstone Arsenal, Mar 56.

Department of the Army Ordnance Corps Report No. 6R3P, Redstone Arsenal, Jul 56.

19. Viegas, J.R. and Horstman, C.C., "Comparison of Multiequation Turbulence Models of Several Shock Separated Boundary-Layer Interaction Flows," AIAA Paper 78-1165, Seattle WA, Jul 78.

20. Needham, D.A. and Stollery, J.L., "Boundary Layer Separation in Hypersonic Flow," AIAA Paper 66-455, Los Angeles CA, Jun 66.

21. Syvertson, C.A. and Dennis, D.H., "A Second-Order Shock-Expansion Method Applicable to Bodies of Revolution Near Zero Lift," NACA Report 1328, 57.

22. Ames Research Staff, "Equations, Tables, and Charts for Compressible Flow", NACA Rep. 1135, 53.

23. Dennis, D.H., "The Effects of Boundary-Layer Separation Over Bodies of Revolution with Conical Tail Flares", NACA Research Memorandum, RM A57I30, Dec. 57.

24. National Research Council, Aeronautics and Space Engineering Board Committee on Computational Aerodynamics Simulation Technology Development, "The Influence of Computational Fluid Dynamics on Experimental Aerospace Facilities - A Fifteen Year Projection", National Academy Press, Washington, D.C., 83.

TABLE 1. EFFECT OF SMOOTHING PARAMETERS ON SEPARATION

INCREMENTAL SMOOTHING PARAMETERS		ARTIFICIAL VISCOSITY SMOOTHING PARAMETERS		FLARE ANG. (ATTACHED)		FLARE ANG. (SEPARATED)	
EPSA	EPSB	SMU (EXPLICIT)	SMUIN (IMPLICIT)	LAM.	TURB.	LAM.	TURB.
2	2	2	4	8.6°	21.5°	10.8°	26.8°
15	15	2	4	7.0°	20.0°	8.0°	21.0°
15	15	15	3	8.0°	21.0°	9.0°	22.0°
25	25	2	4	10.8°	26.6°	12.0°	26.0°

laminar $Re_L = 4.0 \times 10^5$

turbulent $Re_L = 1.5 \times 10^6$

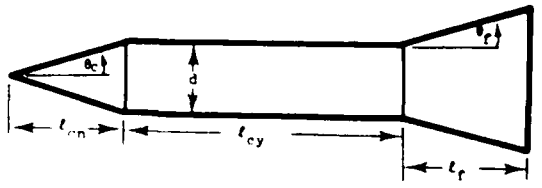

Separation Study

$\theta_c = 10°$

θ_f = 7.00 to 13.42° (laminar)
21.5° to 26.00° (turbulent)

$\ell_{cn} = 2.5$ d

ℓ_{cy} = 2.75 to 11.5 d (laminar)
2.4 to 8.0 d (turbulent)

Aerodynamic Study

$\theta_c = 22.5°$

θ_f = 5° to 20°

$\ell_{cn} = 1.2$ d

$\ell_{cy} = 1, 2, 4$ d

ℓ_f = 1.2 to 4.8 d

Fig. 1 Cone-Cylinder-Flare Geometry.

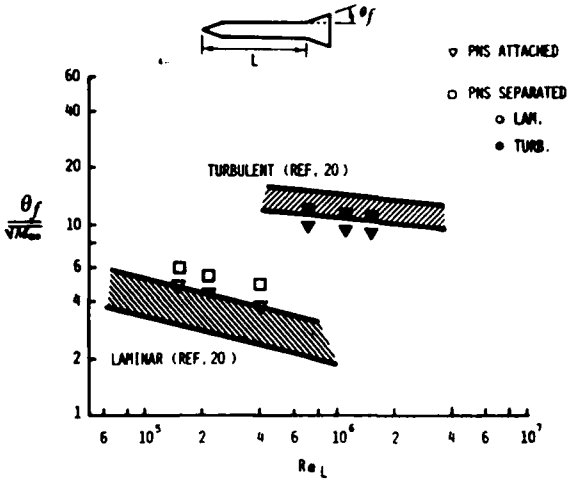

Fig. 2 Correlation of Incipient Separation.

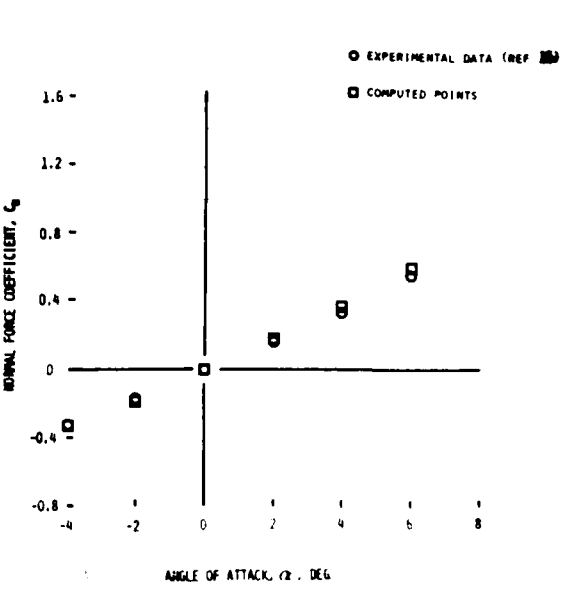

Fig. 3 Normal Force Coefficient vs Angle of Attack.

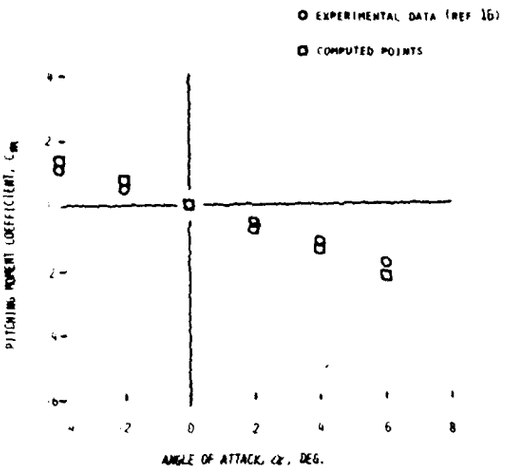

Fig. 4 Pitching Moment Coefficient vs Angle of Attack.

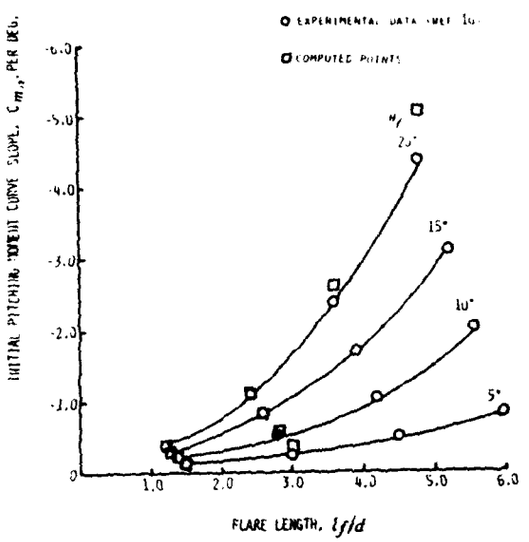

Fig. 6 Initial Pitching Moment Curve Slope vs Flare Length.

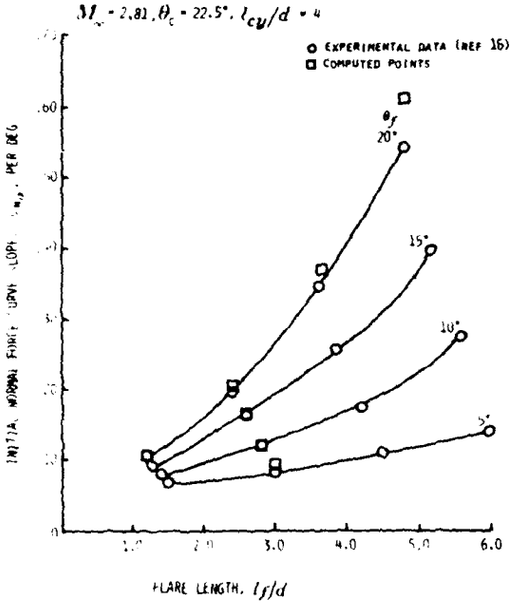

Fig. 5 Initial Normal Force Curve Slope vs Flare Length.

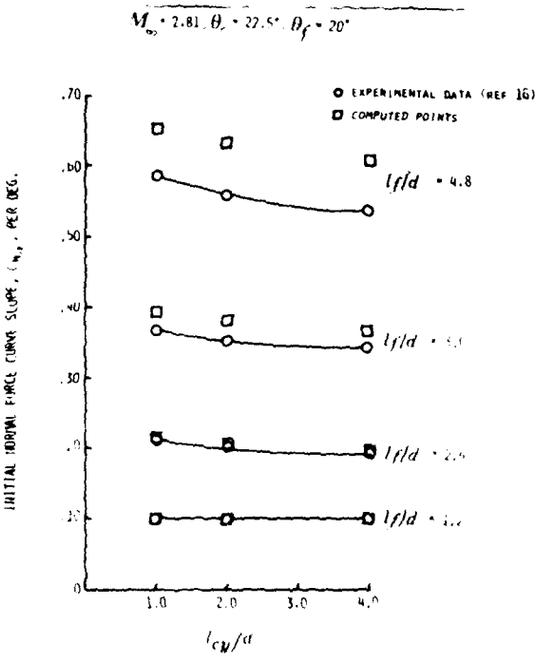

Fig. 7 Initial Normal Force Curve Slope vs Cylinder Length.

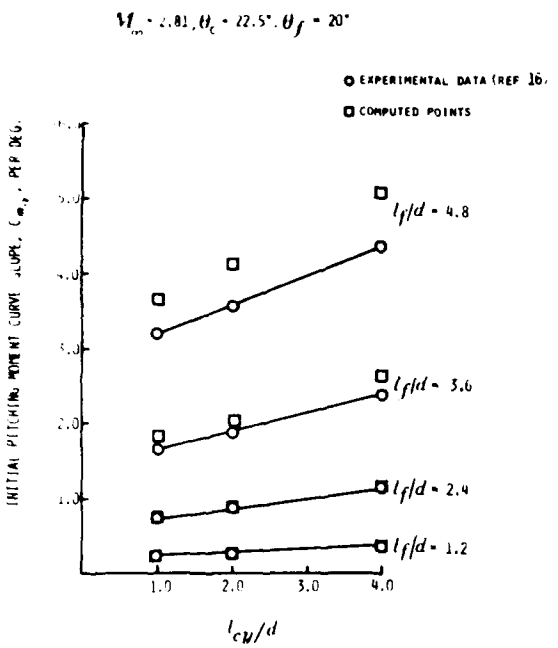

Fig. 8 Initial Pitching Moment Curve Slope vs Cylinder Length.

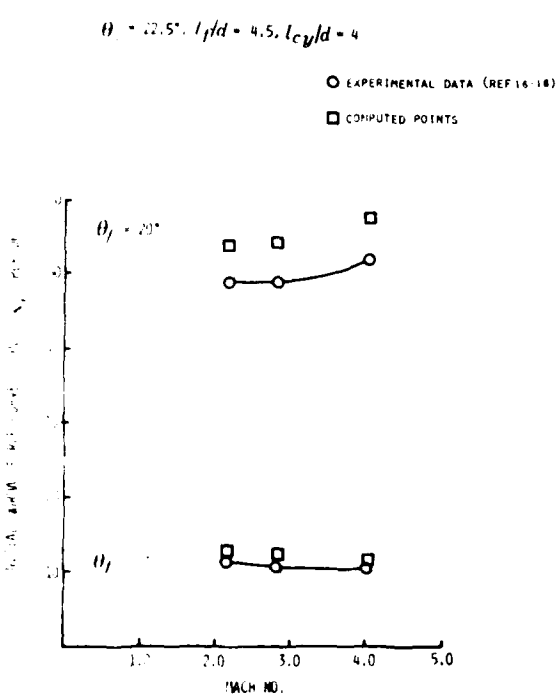

Fig. 9 Initial Normal Force Curve Slope vs Mach Number.

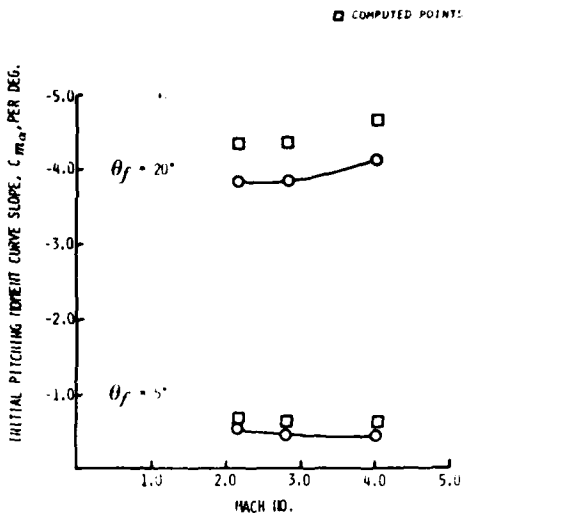

Fig. 10 Initial Pitching Moment Slope vs Mach Number.

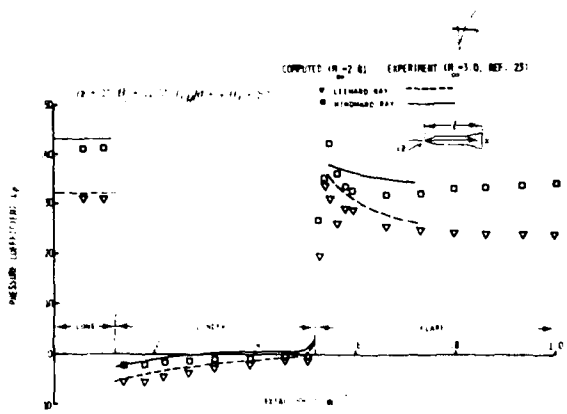

Fig. 11 Pressure Coefficient vs Axial Position.

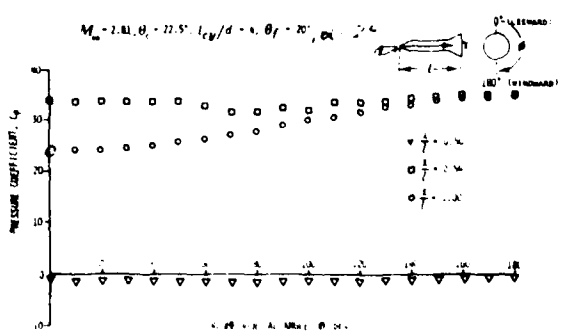

Fig. 12 Pressure Coefficient vs Circumferential Angle.

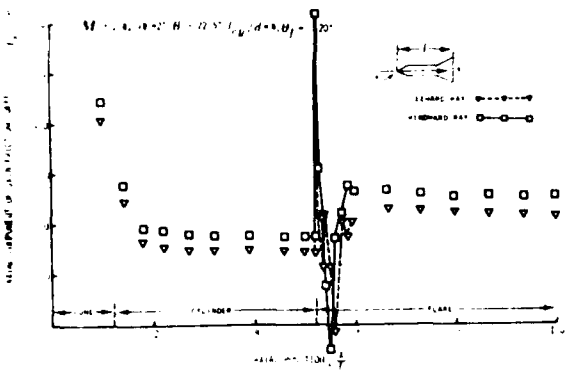

Fig. 13 Axial Component of Skin Friction vs Axial Position.

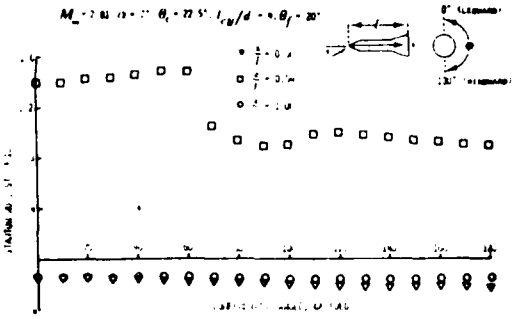

Fig. 16 Stanton Number vs Circumferential Angle.

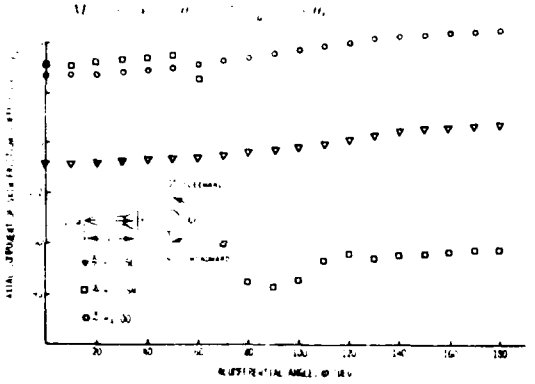

Fig. 14 Axial Component of Skin Friction vs Circumferential Angle.

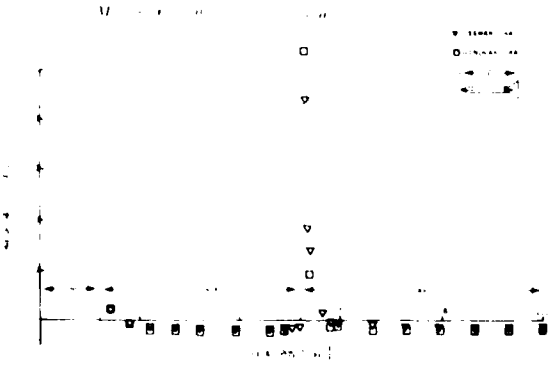

Fig. 15 Stanton Number vs Axial Position.

END

FILMED

5-86

DTIC